geosciences

MDPI

Article

Asymmetric Craters on the Dwarf Planet Ceres—Results of Second Extended Mission Data Analysis

Katrin Krohn [1,*], Ralf Jaumann [1,2], Kai Wickhusen [1], Katharina A. Otto [1], Elke Kersten [1], Katrin Stephan [1], Roland J. Wagner [1], Carol A. Raymond [3] and Christopher T. Russell [4]

1 Institute of Planetary Research, Deutsches Zentrum für Luft- und Raumfahrt, 12489 Berlin, Germany; ralf.jaumann@dlr.de (R.J.); kai.wickhusen@dlr.de (K.W.); katharina.otto@dlr.de (K.A.O.); elke.kersten@dlr.de (E.K.); katrin.stephan@dlr.de (K.S.); roland.wagner@dlr.de (R.J.W.)
2 Institute of Geological Sciences, Planetary Sciences and Remote Sensing, Freie Universität Berlin, 12249 Berlin, Germany
3 Jet Propulsion Laboratory, California Institute of Technology, Pasadena, CA 91109, USA; carol.a.raymond@jpl.nasa.gov
4 Institute of Geophysics and Planetary Physics, University of California, Los Angeles, CA 90095-1567, USA; ctrussell@igpp.ucla.edu
* Correspondence: katrin.krohn@dlr.de; Tel.: +49-30-6705-5683

Received: 13 August 2019; Accepted: 4 November 2019; Published: 12 November 2019

Abstract: After almost three years of successful operation on Ceres, the Dawn spacecraft entered its last orbits around the dwarf planet and obtained a set of high-resolution images of 3 to 5 m/pixel. These images reveal a variety of morphologic features, including a set of asymmetric crater morphologies as observed earlier in the mission on the asteroid Vesta. We identified 269 craters, which are located between 60° N to 60° S latitude and 197° E to 265° E longitude, and investigated their morphological characteristics using a digital terrain model (DTM). These craters range in diameter from 0.30 to 4.2 km, and exhibit a sharp crater rim on the uphill side and a smooth one on the downhill side. We found that all asymmetric craters are formed on a sloping surface with the majority appearing at slope angles between 5 and 20 degrees. This implies that, as observed on Vesta, the topography is the main cause for these asymmetries.

Keywords: crater formation on small bodies; cratering processes; influence of slopes; asteroids; dwarf planets; asymmetrical cratering; XM2

1. Introduction

Most craters on planetary surfaces have a circular shape, but on smaller airless bodies, such as the Moon [1], Vesta [2,3], and Lutetia [4,5], craters with a specific asymmetric shape are observed. The craters show a sharp uphill crater rim and a smooth downhill crater rim. The origin of asymmetric craters is manifold, and in most cases, is not fully solved yet. Generally, impact crater formation is discussed for impacts into more or less planar surfaces, but there are theories that asymmetries in the crater forms are a result of projectile trajectory [6–8]. An asymmetric ejecta distribution could be due to shallow impact angles. The shallower the impact angle, the more elongated is the crater [7,8]. Furthermore, the topography [9] or the heterogeneity of stratigraphy [10,11] can play a role in the formation process of the asymmetry of craters. Additionally, the initial circular impact crater structure could be overprinted by post-impact modification, such as volcanism [12], tectonics [13], or erosion [14], and could change the circular structure into an asymmetric shape.

Before departing to the dwarf planet Ceres, the Dawn spacecraft [15] characterized the geology, mineralogical composition, topography, shape, and internal structure of Vesta [2]. One of the interesting outcomes of this research was the discovery of asymmetric craters on the surface of the asteroid [2,3]. Three-dimensional hydrocode simulations of those craters on Vesta revealed that the shape is caused by the formation of craters on slopes [3]. That study [3] showed that the slope prevents the deposition of ejected material in uphill direction and results in a larger accumulation of ejecta within the crater and on the downhill crater rim.

In this paper, we will analyze and discuss the formation processes for the asymmetries of craters on Ceres in comparison to our findings for Vesta.

2. Data and Methods

After three years of successful operation on Ceres and two extended missions, the Dawn mission ended on 1 November 2018. Between March 2015 and November 2018, the Dawn spacecraft was in orbit around Ceres, obtaining datasets from three instruments (Framing Camera (FC) [16], Visible and InfraRed (VIR) spectrometer [17], Gamma Ray and Neutron Detector (GRaND) [18]) in different orbits with varying spacial resolutions.

The last orbit, i.e., the second extended, mission (XM2) at Ceres was approved to obtain new high-priority science data until the spacecraft ran out of hydrazine, used for the altitude control of the spacecraft. The science cases comprised the detection of elemental concentrations with high sensitivity and spatial resolution, and furthermore, the investigation of possible cryovolcanic deposits including the identification of their source and the driving cryovolcanic processes [19]. However, the acquired XM2 FC images also revealed a so far undetected asymmetric crater shape in case of small craters on Ceres.

During the XM2 mission, Dawn reached a resonant, eccentric orbit with a pericenter at 35 km altitude, allowing for the obtainment of the highest-resolution Framing Camera images of the entire Dawn mission [20]. Since asymmetric craters are first recognized in XM2 data, we analyzed all available data of the Dawn Framing Camera (FC) data from the second extended mission with a spatial resolution of 3 to 5 m/pixel. The data cover Ceres' surface in the range of 60° N to 60° S latitude and 197° E to 265° E longitude, focusing on the observation of the prominent impact crater Occator and parts of the Urvara region (Figures 1 and 2).

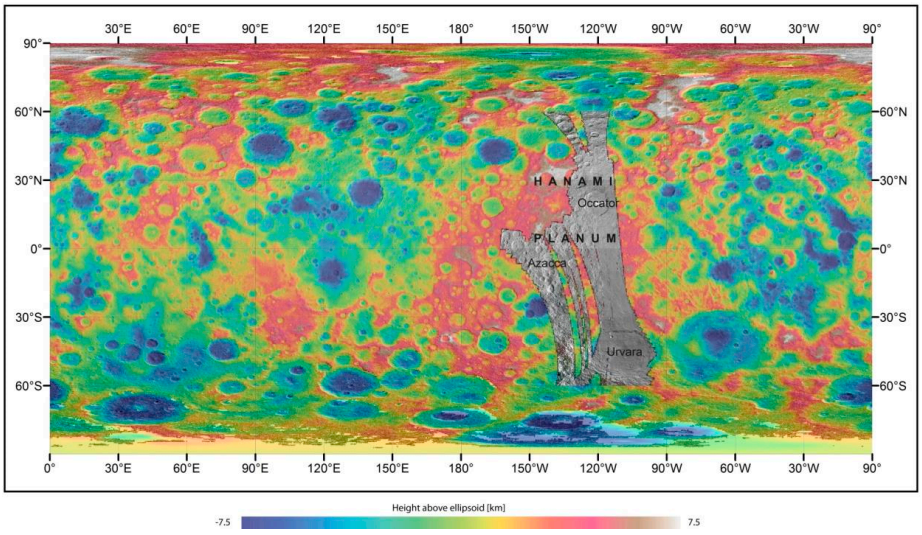

Figure 1. Global map of Ceres with overlaying (Digital Terrain Model) DTM. The clear filter mosaic shows the obtained (Extended Mission 2) XM2 data. The figure shows no obvious elevation differences that distinguish between highlands and lowlands, except for Hanami Planum.

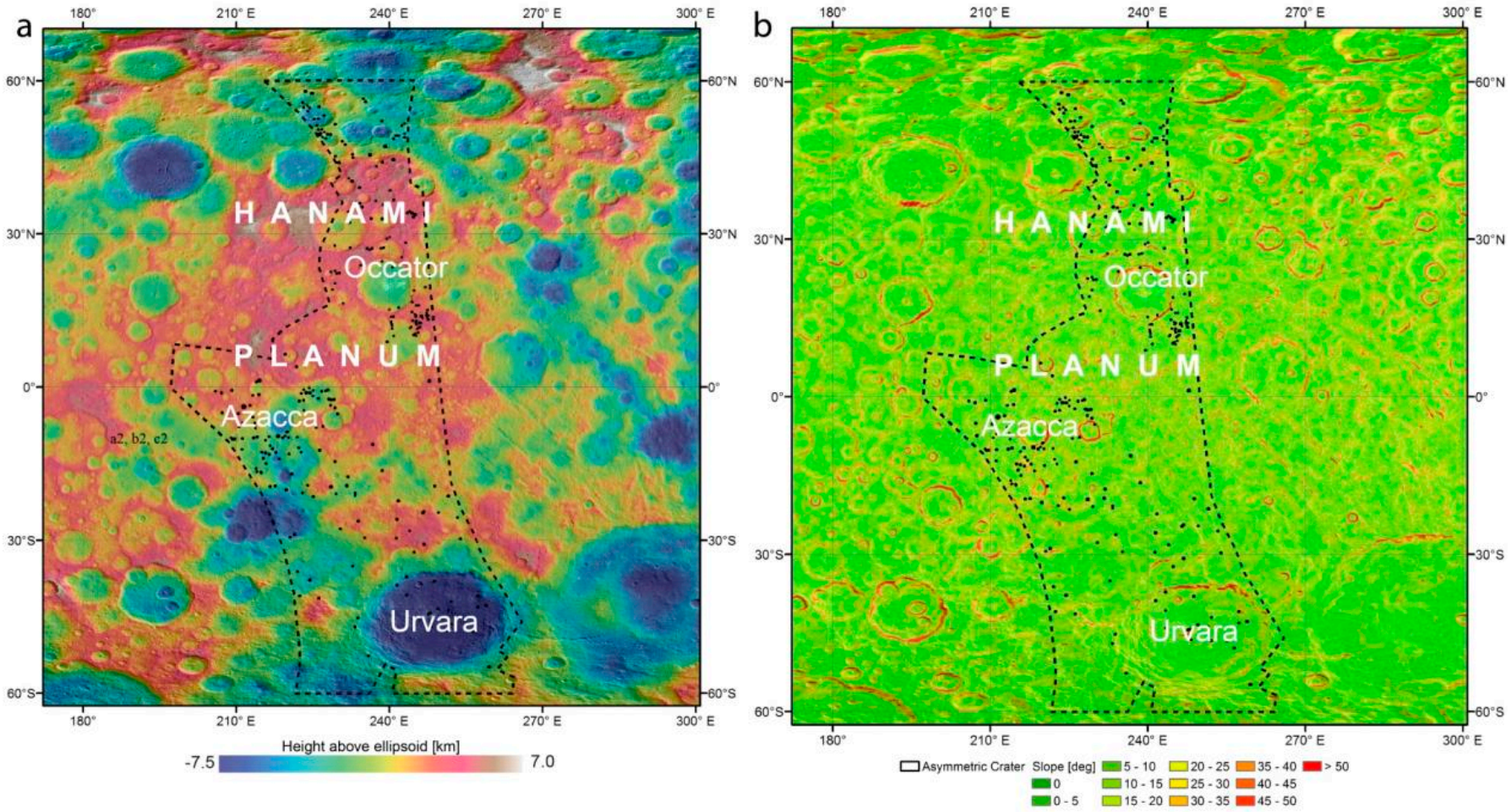

Figure 2. Distribution of asymmetric craters (**a**) on an elevation map of the study area. (**b**) The slope map shows low slope variations on Ceres. The majority of slope angles are < 20 degrees. The craters are displayed by a black circle; the black dotted line indicates the approximate border of the XM2 data (see Figure 1 for details).

In order to analyze the morphology of these craters, we made use of a digital terrain model (DTM) derived from stereo-photogrammetrically processed FC High Altitude Mapping Orbit (HAMO) data with a spatial resolution of ~135 m/pixel [21]. Where available, we also used the DTMs resulting from the Low Altitude Mapping Orbit (LAMO) data with a spatial resolution of 32 m/pixel [21,22].

We identified and mapped the outline of each asymmetric crater using ESRI´s software package ArcGIS 10.5.1. The crater diameters were measured with the help of CraterTools [23] from rim crest to rim crest. The morphology of asymmetric craters is described by asymmetrical crater shapes on sloping surfaces with sharp and smooth crater rims, asymmetric interior morphology, and ejecta distribution [3]. Therefore, to obtain the most accurate impression of the surface, we generated a slope map from the HAMO DTM with the ArcGIS slope map tool using the DTMs. The slope is calculated by the maximum rate of change in value from each cell to its neighbors. Due to the resolution of 3 to 5 m/pixel for the FC XM2 data, we can identify asymmetrical craters with diameters down to 300 m with sufficient accuracy.

3. Results

Impact craters are the most prevalent geomorphologic features on Ceres. Craters on Ceres show a large variety of crater morphologies [24,25], including bowl-shaped craters, polygonal craters [25,26], floor-fractured craters [25,27], secondary craters, crater chains, and craters with terraces, central peaks, smooth crater floors [25], flow-like features [25,28–31], and bright spots [25,32–34].

The analysis of XM2 data reveals 269 craters (Figure 3) with a crater similar to asymmetric craters observed on Vesta, the Moon, and Lutetia. A full list of all 269 asymmetric craters is given in the Supplemental Material (S1). They show an asymmetric crater interior with an oblique and a shallower side, as well as an asymmetric ejecta distribution. The crater show a semi-circular sharp and well-formed rim on the uphill side, and a smooth rim on the downhill side (Figure 3a). Due to local accumulation of material covering the downhill crater rim, the rim crest is not clearly detectable. Ejecta deposits are only sporadically detected in thin layers on the uphill rim. The majority of the upslope inner crater walls show mass wasting features. Most asymmetric craters on Ceres show a relative straight border in the lower third through the crater, separating the oblique from the shallower crater floor (Figure 4). The uphill crater wall shows a smooth texture with a downslope movement of material accumulated at the border.

Some craters show a slightly more elongated shape in uphill direction than the other craters. The uphill rim seems to merge with the slope. The downhill rim shows a less elevated rim than the other craters, but with the same ejecta and mass wasting material distribution. Nevertheless, the craters also show the border between the steeper and the shallower crater parts. However, the crater floor appears wider than the others (Figure 3c). The projectile forming this crater seems to have impacted on the slope crest (Figure 3c).

The crater diameters of asymmetric craters on Ceres vary from 0.30 to 4.2 km, with a mean diameter of 0.98 km. Overall, the craters are more or less homogeneously distributed over the study area. We only see a cluster of about 57 asymmetric craters southeast of Occator and about 90 craters in the south, southwest, and northeast of the Azacca crater (Figure 2). The craters around Azacca are preferentially found in the lows adjacent to the topographically high region named Hanami Planum. Twenty-one asymmetric craters are also found all over the crater floor of the huge Urvara basin (~170 km diameter).

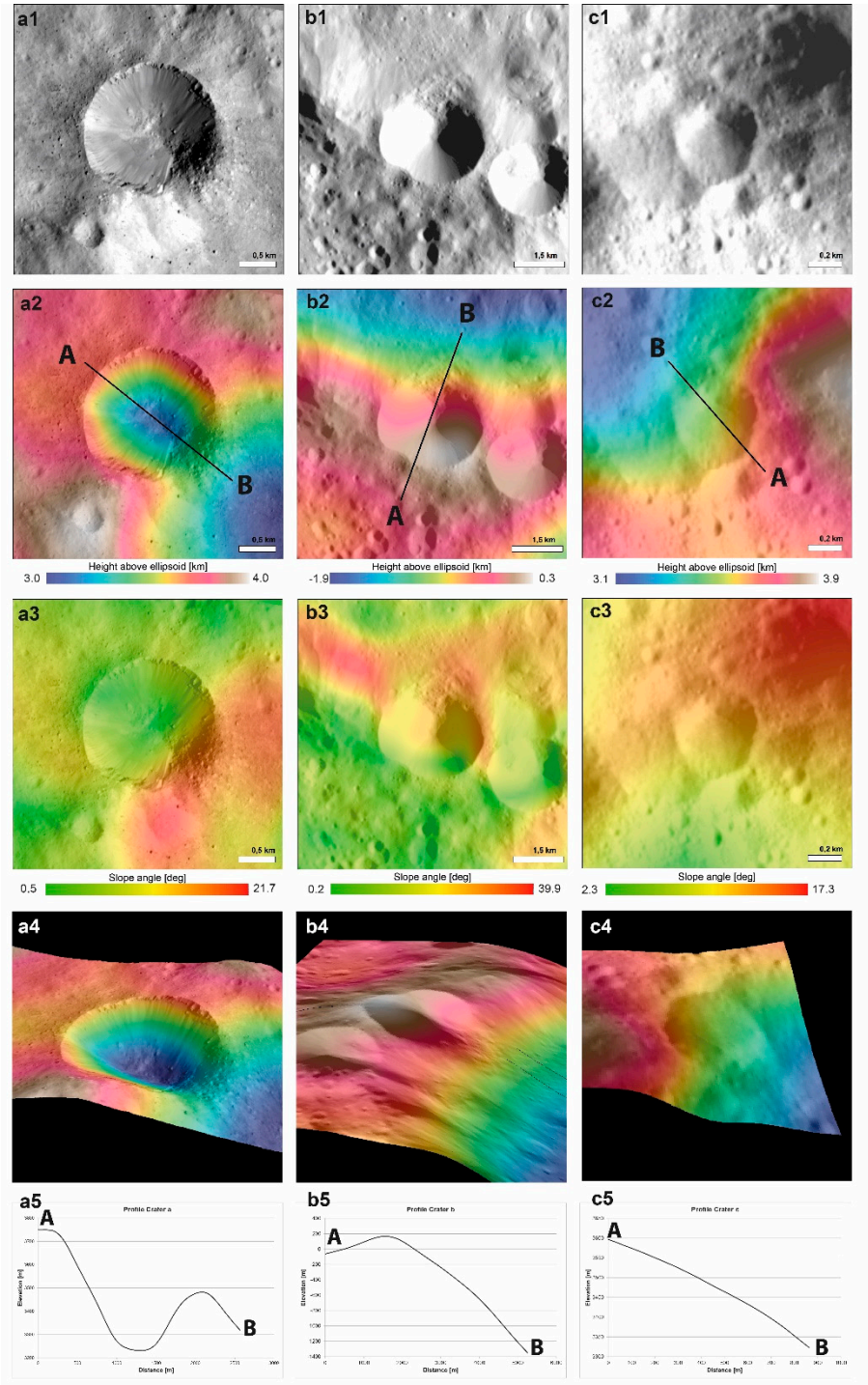

Figure 3. Examples of asymmetric craters on Ceres. (**a1**) Clear filter image of an unnamed crater at 245.96° E and 12.57° N; and (**b1**) clear filter image of an unnamed crater at 218.18° E and 9.55° S show the typical asymmetric crater form, with a sharp uphill rim and a smooth downhill rim, covered with mass wasting material from the crater flanks. There are little ejecta visible above the uphill rim. The DTM (**a2**) and slope map (**a3**) of the crater shows that the crater was formed on a slope crest. (**b2**) DTM and (**b3**) slope map shows the formation on a slope. (**c1**) Clear filter image of an unnamed crater at 245.16° E and 12.63° N shows a more elongated shape in the uphill direction than the other craters. The uphill rim seems to merge with the slope. (**c2**) DTM of 245.16° E and 12.63° N. (**c3**) Slope map of 245.16° E and 12.63° N. (**a4**,**b4**,**c4**) Perspective views of the particular craters; the elevation is the same as in (**a2**,**b2**, **c2**). (**a5**,**b5**,**c5**) Profiles of the particular craters; start and end is provided in (**a2**,**b2**,**c2**).

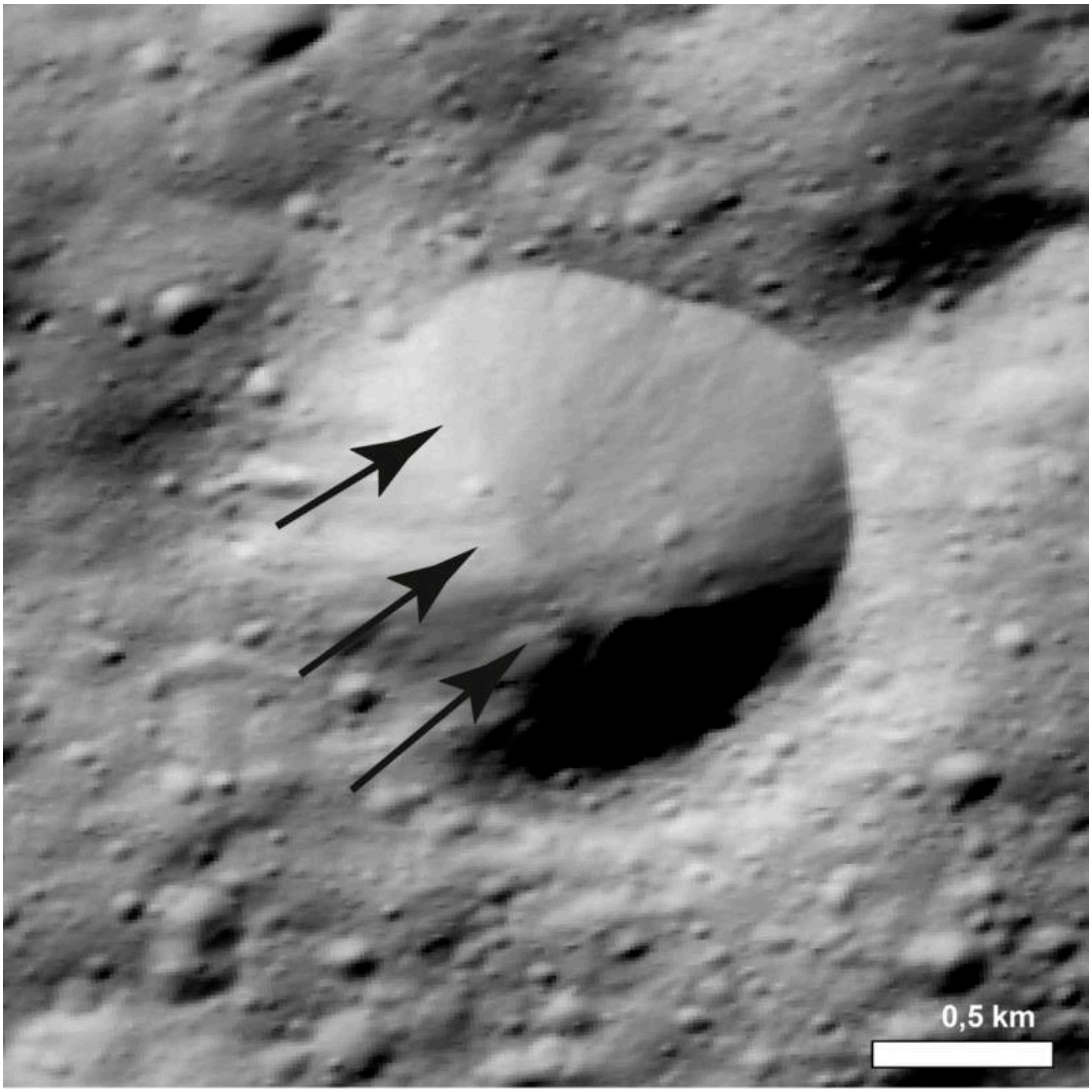

Figure 4. Asymmetric crater at 232.67° E and 40.36° N, showing a relatively straight border in the lower third of the crater, separating the oblique from the shallower crater floor (black arrows).

Figure 5 shows the crater frequency ratio of asymmetric craters of Ceres and Vesta with respect to the different slope angles. The value 1 corresponds to the average asymmetric crater distribution over the total area of the particular body. The average is defined by percent crater on each slope divided by percent slope angle area of each slope. The occurrence of asymmetric craters on low slope angles is significantly lower than on high slope angles. On Ceres the figure shows that asymmetric craters on slope angles between 5 to 10 degrees as well over 20 degrees are on average. Asymmetric craters on slope angles from 10 to 20 degrees are significantly above the average. Asymmetric craters on Vesta on slope angles between 0 to 10 degrees are significantly below the average, whereas craters over 10 degrees are significantly above the average [3].

Figure 6 shows that on Ceres the crater frequency depending on diameters in correlation with the particular slope angle. Large craters with diameters > 2.4 km only occur on slopes angles > 5 degrees. For diameters from 0.4 to 1.4 km, we see the highest amount of craters on all slope angles, followed by a continuous decrease within creasing crater diameter on both bodies. For Ceres this is consistent with the global crater catalog of [24], which shows different crater morphologies besides asymmetric craters with diameters ≥ 1 km. The majority of craters in this catalog exhibits diameters between 1 and

1.5 km, and decreases with increasing crater diameter [24]. The general fall-off in the appearance of asymmetric craters with increasing diameter fits this global trend of total craters.

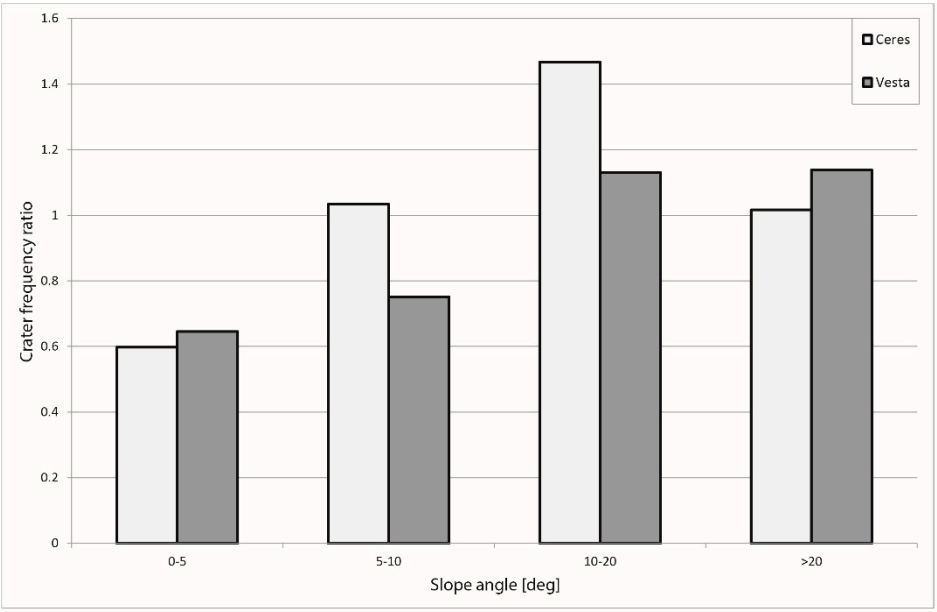

Figure 5. This figure shows the crater frequency ratio of asymmetric craters on the different slope angles in comparison with Vesta (modified after [3]). Most craters on Ceres are on average or above average slope angles between 5 and > 20 degrees. Most craters on Vesta over 10 degrees are significantly above the average.

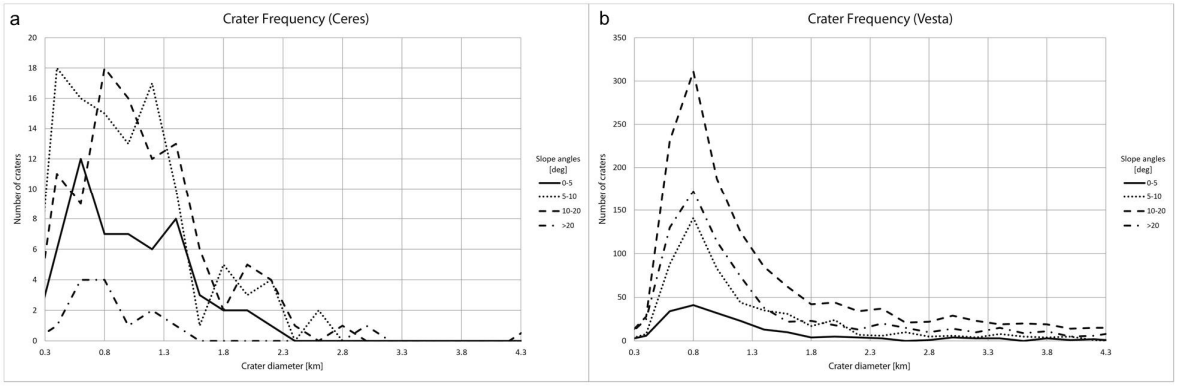

Figure 6. Crater frequency over diameters in correlation with the slope angles on Ceres (**a**) and Vesta (**b**) (modified after [3]). The figure shows the highest amount of craters for diameters from 0.4 to 1.4 km, followed by a continuous decrease. This general fall-off fits the global trend of total craters.

4. Discussion and Conclusions

On Vesta, the distinct morphology of asymmetric craters has been attributed to impacts on slopes [3]. Furthermore, numerical modeling [3,9,35] shows that the formation of asymmetric craters is significantly affected by the topography with the best results given by a 1-km sized projectile hitting a slope at its base and the impactor trajectory in this case directed towards the slope with an oblique angle of incidence of 15 degrees [3].

The shape of an impact crater, and mainly its ejecta distribution, is the effect of a multifaceted interaction of topographic setting [9]. The combination of impact energy, which is caused by the size, density, and velocity of the projectile, the oblique angle of incidence, the impact position in relation to the topography, and the properties of the target material, plays an important role in the formation of

the asymmetry of craters. Until the end of the excavation stage, gravitational forces are too low to significantly influence the cratering process, and thus, the excavation is only dominated by inertial forces. The transient crater is therefore similar in shape to an impact on a planar surface. However, in the continuing cratering process, gravity becomes more important, and the ejecta curtain angle in the uphill direction is influenced by the slope. Thus, when the ejecta curtain collapses, the uppermost material from the slope is deposited inside the crater and results in a sharp edge of the crater in the uphill direction [3] (Figures 3 and 4). Steep slopes and/or low impact angles can also cause the deposition of uphill-directed ejecta outside the downhill crater rim. Consequently, only few or no ejecta deposits are detected over the uphill rim of asymmetric craters.

Asymmetric craters on Vesta are characterized by a sharp edge on the uphill side, a smooth rim and material accumulation downhill, with little or no ejecta deposits on the uphill side [3]. The craters on Ceres look quite similar. They also show a sharp crater rim with little or no ejecta on the uphill side and a smooth-material-covered crater rim on the downhill side. On Vesta, the diameters of asymmetric craters range from 0.3 to 42.6 km on slope angles from > 5 to over 20 degrees, with a maximum appearance on slope angles > 10 degrees [3] (Figure 6). On Ceres, however, we observed asymmetric crater diameters varying from 0.30 to 4.2 km on slope angles between 5 and 20 degrees, with a maximum appearance on slope angles between 5 to 10 degrees. Only a few craters are found on slope angles over 20 degrees (Figure 6). The crater frequency ratio is similar on both bodies, indicating a similar formation process for the asymmetries due to slope angles.

However, why did not we see any bigger asymmetric craters on Ceres?

Ceres reveals ~15 km of total relief (−7.5–7.5 km), derived from stereo-photogrammetric analysis referenced to the mean radius [25]. For comparison, Vesta exhibits a total relief of ~41 km [2], which is significantly higher than on Ceres. In contrast to Vesta, Ceres shows no obvious elevation differences that distinguish the highlands from the lowlands, except for one discrete topographically high region, named Hanami Planum [36] (Figures 1 and 2). Thus, extreme topographic variations on Vesta have caused many craters to be formed on slopes. Generally, the topographic differences on Ceres are less distinctive and not as steep as on Vesta. The only region where steeper slopes are expected is Hanami Planum. However, while the rim of Hanami Planum shows parts of a shallow sloped terrain (Figure 2b), the rim is also affected by large craters, which would obliterate the slopes significantly due to their size and mass, and which might have eliminated them. This effect is also expected for low-altitude slopes. Additionally, low-altitude slopes would be preferentially destroyed as they become buried by the ejecta of large craters >20 km. Therefore, the low topographic variations with low slope angles could have limited the crater size formation on the slopes.

Additionally, Ceres consists of a shell, dominated by an ice-rock mixture [37–39] and ammoniated phyllosilicates [32,40,41]. The volatile-rich outer layer is supposed to have an average thickness of about 41.0 + 3.2–4.7 km [42,43]. Impacts into such ice-rock layers may be modified by melting of material and will not necessarily show a clear asymmetry of the crater rims. The Occator region, in light of the XM2 data, is supposed to contain subsurface ice at a relatively shallow depth, below a thin protective layer of regolith [31,38,39,44]. Thus, an accurate identification of asymmetric craters can only be observed on solid rocks. Many craters within Occator with a mean diameter of ~710 m occur as ring-mold craters, which are thought to be formed by impacting into a regolith-covered ice layer. Bowl-shaped craters in this area are smaller, with a mean of ~366 m, indicating that the overlying regolith layer is only several tens of meters thick [44]. This would lead to the assumption that craters, especially in this region, have to be smaller than ring-mold craters to develop asymmetries. Such craters, however, cannot be clearly identified due to the spatial resolution of the data.

Another possible explanation for the asymmetries of the craters could be erosion or tectonic processes. Erosional processes on Ceres are mainly caused by seismic shaking due to impact events, or flow features such as cryovolcanic flows [28] and ground-ice flows [29]. However, those flows would be characterized by a more compact morphology with relatively smooth surfaces and no loose material, as on the downhill rim of the studied craters. Moreover, the material of uphill ejecta, if present,

and downhill material seem to be deposited simultaneously. This means that they were not influenced by post-emplacement modifications.

We also see no signs of recent tectonic activity near the asymmetric craters, such as an active uplift of Hanami Planum, which might cause the uplift of crater parts and mass wasting material, flowing down the crater walls and remaining on the downhill crater rim. However, Hanami Planum appears relatively old. The surface is densely cratered and the flanks showing no young landslide as in the flanks of Ahuna Mons [45]. On the contrary, the asymmetric craters appear relatively young.

In conclusion, this work shows that the three prominent features of the asymmetric craters on Ceres are a sharp uphill crater rim, a smooth downhill rim with mass wasting material, and little or no ejecta deposits on the uphill side of craters formed on a slope. Although there are only small craters showing such asymmetries, we conclude that topography is the main cause for the asymmetries observed in these craters on Ceres. Larger craters with asymmetries are unlikely due to the low topographic variations on Ceres.

Supplementary Materials: The following are available online at http://www.mdpi.com/2076-3263/9/11/475/s1, Table S1: List of all asymmetric craters on Ceres used in our study.

Author Contributions: Conceptualization, K.K. and R.J.; Methodology, K.K. and K.W.; Investigation, K.K.; Data Curation, K.K. and E.K.; Writing—Original Draft Preparation, K.K.; Writing—Review and Editing, R.J., K.W., K.A.O., K.S., and R.J.W.; Visualization, K.K. and K.W.; Supervision, R.J.; Project Administration, C.A.R. and C.T.R.

Funding: This research received no external funding.

Acknowledgments: We thank the Dawn team for the development, cruise, orbital insertion, and operations of the Dawn spacecraft at Ceres. Portions of this work were performed at the DLR Institute of Planetary Research, at the Jet Propulsion Laboratory (JPL) under contract with NASA, and the German Aerospace Center (DLR). Dawn data are archived with the NASA Planetary Data System https://sbn.psi.edu/pds/resource/dawn/dwncfcL1.html.

Conflicts of Interest: The authors declare no conflict of interest.

References

1. Plescia, J.B. Impacts on Sloping Surfaces: Lunar Examples. *Meteorit. Planet. Sci. Suppl.* **2012**, *75*, 5318.
2. Jaumann, R.; Williams, D.A.; Buczkowski, D.L.; Yingst, R.A.; Preusker, F.; Hiesinger, H.; Schmedemann, N.; Kneissl, T.; Vincent, J.B.; Blewett, D.T.; et al. Vesta's shape and morphology. *Science* **2012**, *336*, 687–690. [CrossRef] [PubMed]
3. Krohn, K.; Jaumann, R.; Elbeshausen, D.; Kneissl, T.; Schmedemann, N.; Wagner, R.; Voigt, J.; Otto, K.; Matz, K.D.; Preusker, F.; et al. Asymmetric craters on Vesta: Impact on sloping surfaces. *Planet. Space Sci.* **2014**, *103*, 36–56. [CrossRef]
4. Massironi, M.; Marchi, S.; Pajola, M.; Snodgrass, C.; Thomas, N.; Tubiana, C.; Baptiste Vincent, J.; Cremonese, G.; Da Deppo, V.; Ferri, F.; et al. Geological map and stratigraphy of asteroid 21 Lutetia. *Planet. Space Sci.* **2012**, *66*, 125–136. [CrossRef]
5. Thomas, N.; Barbieri, C.; Keller, H.U.; Lamy, P.; Rickman, H.; Rodrigo, R.; Sierks, H.; Wenzel, K.P.; Cremonese, G.; Jorda, L.; et al. The geomorphology of (21) Lutetia: Results from the OSIRIS imaging system onboard ESA's Rosetta spacecraft. *Planet. Space Sci.* **2012**, *66*, 96–124. [CrossRef]
6. Elbeshausen, D.; Wünnemann, K.; Collins, G.S. Scaling of oblique impacts in frictional targets: Implications for crater size and formation mechanisms. *Icarus* **2009**, *204*, 716–731. [CrossRef]
7. Gault, D.E.; Wedekind, J.A. Experimental Studies of Oblique Impact. In Proceedings of the Lunar and Planetary Science Conference Proceedings, Houston, TX, USA, 13–17 March 1978; pp. 3843–3875.
8. Elbeshausen, D.; Wünnemann, K.; Collins, G.S. The transition from circular to elliptical impact craters. *J. Geophys. Res.* **2013**, *118*, 2295–2309. [CrossRef]
9. Elbeshausen, D.; Wünnemann, K. The Effect of Target Topography and Impact Angle on Crater Formation—Insight from 3D Numerical Modelling. In Proceedings of the Lunar and Planetary Institute Science Conference Abstracts, The Woodlands, TX, USA, 7–11 March 2011; p. 1778.
10. Collins, G.S.; Morgan, J.; Barton, P.; Christeson, G.L.; Gulick, S.; Urrutia, J.; Warner, M.; Wünnemann, K. Dynamic modeling suggests terrace zone asymmetry in the Chicxulub crater is caused by target heterogeneity. *Earth Planet. Sci. Lett.* **2008**, *270*, 221–230. [CrossRef]

11. Gulick, S.P.S.; Barton, P.J.; Christeson, G.L.; Morgan, J.V.; McDonald, M.; Mendoza-Cervantes, K.; Pearson, Z.F.; Surendra, A.; Urrutia-Fucugauchi, J.; Vermeesch, P.M.; et al. Importance of pre-impact crustal structure for the asymmetry of the Chicxulub impact crater. *Nat. Geosci.* **2008**, *1*, 131–135. [CrossRef]
12. Schultz, P.H. *Moon Morphology: Interpretations Based on Lunar Orbiter Photography*; University of Texas Press: Austin, TX, USA, 1976.
13. Gurov, E.P.; Koeberl, C.; Yamnichenko, A. El'gygytgyn impact crater, Russia: Structure, tectonics, and morphology. *Meteorit. Planet. Sci.* **2007**, *42*, 307–319. [CrossRef]
14. Simonds, C.H.; Kieffer, S.W. Impact and volcanism—A momentum scaling law for erosion. *J. Geophys. Res.* **1993**, *98*, 14321. [CrossRef]
15. Russell, C.T.; Raymond, C.A. The Dawn mission to Vesta and Ceres. *Space Sci. Rev.* **2011**, *163*, 3–23. [CrossRef]
16. Sierks, H.; Keller, H.U.; Jaumann, R.; Michalik, H.; Behnke, T.; Bubenhagen, F.; Büttner, I.; Carsenty, U.; Christensen, U.; Enge, R.; et al. The Dawn Framing Camera. *Space Sci. Rev.* **2011**, *163*, 263–327. [CrossRef]
17. De Sanctis, M.C.; Coradini, A.; Ammannito, E.; Filacchione, G.; Capria, M.T.; Fonte, S.; Magni, G.; Barbis, A.; Bini, A.; Dami, M.; et al. The VIR Spectrometer. *Space Sci. Rev.* **2011**, *163*, 329–369. [CrossRef]
18. Prettyman, T.H.; Feldman, W.C.; McSween, H.Y.; Dingler, R.D.; Enemark, D.C.; Patrick, D.E.; Storms, S.A.; Hendricks, J.S.; Morgenthaler, J.P.; Pitman, K.M.; et al. Dawn's Gamma Ray and Neutron Detector. *Space Sci. Rev.* **2011**, *163*, 371–459. [CrossRef]
19. Raymond, C.; Russell, C.T.; Pieters, C.; Mc Cord, T.B.; Castillo-Rogez, J.; McSween, H.; Marchi, S.; De Sanctis, M.C. Origins of Vesta and Ceres and Implications for Planetesimal Diversity. In Proceedings of the 42nd COSPAR Scientific Assembly, Pasadena, CA, USA, 14–22 July 2018.
20. Raymond, C.A.; Castillo, J.C.; Russell, C.T.; De Sanctis, M.C.; Nathues, A.; Prettyman, T.H.; Park, R.S.; Rayman, M.; Polanskey, C.A.; Joy, S.P.; et al. Dawn's second extended mission at Ceres: The final harvest. In Proceedings of the AGU Fall Meeting Abstracts, Washington, DC, USA, 10–14 December 2018; Volume 24.
21. Preusker, F.; Scholten, F.; Matz, K.-D.; Elgner, S.; Jaumann, R.; Roatsch, T.; Joy, S.P.; Polanskey, C.A.; Raymond, C.A.; Russell, C.T. Dawn at Ceres—Shape Model and Rotational State. In Proceedings of the Lunar and Planetary Science Conference, The Woodlands, TX, USA, 21–25 March 2016; p. 1954.
22. Roatsch, T.; Kersten, E.; Matz, K.-D.; Preusker, F.; Scholten, F.; Elgner, S.; Schroeder, S.E.; Jaumann, R.; Raymond, C.A.; Russell, C.T. *Dawn Fc2 Derived Ceres Lamo Dtm Spg V1.0, Dawn-A-Fc2-5-Cereslamodtmspg-V1.0*; NASA Planetary Data System: Washington, DC, UAS, 2018.
23. Kneissl, T.; van Gasselt, S.; Neukum, G. Map-projection-independent crater size-frequency determination in GIS environments—New software tool for ArcGIS. *Planet. Space Sci.* **2011**, *59*, 1243–1254. [CrossRef]
24. Gou, S.; Yue, Z.; Di, K.; Liu, Z. A global catalogue of Ceres impact craters ≥ 1 km and preliminary analysis. *Icarus* **2018**, *302*, 296–307. [CrossRef]
25. Buczkowski, D.L.; Schmidt, B.E.; Williams, D.A.; Mest, S.C.; Scully, J.E.C.; Ermakov, A.I.; Preusker, F.; Schenk, P.; Otto, K.A.; Hiesinger, H.; et al. The geomorphology of Ceres. *Science* **2016**, 353. [CrossRef]
26. Otto, K.A.; Jaumann, R.; Krohn, K.; Buczkowski, D.L.; von der Gathen, I.; Kersten, E.; Mest, S.C.; Naß, A.; Neesemann, A.; Preusker, F.; et al. Polygonal Impact Craters on Ceres: Morphology and Distribution. In Proceedings of the 79th Annual Meeting of the Meteoritical Society, Berlin, Germany, 7–12 August 2016; Volume 1921.
27. Buczkowski, D.L.; Sizemore, H.G.; Bland, M.T.; Scully, J.E.C.; Quick, L.C.; Hughson, K.H.G.; Park, R.S.; Preusker, F.; Raymond, C.A.; Russell, C.T. Floor-Fractured Craters on Ceres and Implications for Interior Processes. *J. Geophys. Res.* **2018**, *123*, 3188–3204. [CrossRef]
28. Krohn, K.; Jaumann, R.; Stephan, K.; Otto, K.A.; Schmedemann, N.; Wagner, R.J.; Matz, K.D.; Tosi, F.; Zambon, F.; von der Gathen, I.; et al. Cryogenic flow features on Ceres: Implications for crater-related cryovolcanism. *Geophys. Res. Lett.* **2016**, *43*, 1–10. [CrossRef]
29. Schmidt, B.E.; Hughson, K.H.G.; Chilton, H.T.; Scully, J.E.C.; Platz, T.; Nathues, A.; Sizemore, H.; Bland, M.T.; Byrne, S.; Marchi, S.; et al. Geomorphological evidence for ground ice on dwarf planet Ceres. *Nat. Geosci.* **2017**, *10*, 338–343. [CrossRef]
30. Krohn, K.; Jaumann, R.; Otto, K.A.; Schulzeck, F.; Neesemann, A.; Nass, A.; Stephan, K.; Tosi, F.; Wagner, R.J.; Zambon, F.; et al. The unique geomorphology and structural geology of the Haulani crater of dwarf planet Ceres as revealed by geological mapping of equatorial quadrangle Ac-6 Haulani. *Icarus* **2018**, *316*, 84–98. [CrossRef]

31. Scully, J.E.C.; Buczkowski, D.L.; Raymond, C.A.; Bowling, T.; Williams, D.A.; Neesemann, A.; Schenk, P.M.; Castillo-Rogez, J.C.; Russell, C.T. Ceres' Occator crater and its faculae explored through geologic mapping. *Icarus* **2019**, *320*, 7–23. [CrossRef]
32. de Sanctis, M.C.; Ammannito, E.; Carrozzo, F.G.; Ciarniello, M.; Giardino, M.; Frigeri, A.; Fonte, S.; McSween, H.Y.; Raponi, A.; Tosi, F.; et al. Ceres's global and localized mineralogical composition determined by Dawn's Visible and Infrared Spectrometer (VIR). *Meteorit. Planet. Sci.* **2018**, *53*, 1844–1865. [CrossRef]
33. Ruesch, O.; Quick, L.C.; Landis, M.E.; Sori, M.M.; Čadek, O.; Brož, P.; Otto, K.A.; Bland, M.T.; Byrne, S.; Castillo-Rogez, J.C.; et al. Bright carbonate surfaces on Ceres as remnants of salt-rich water fountains. *Icarus* **2019**, *320*, 39–48. [CrossRef]
34. Stein, N.T.; Ehlmann, B.L.; Palomba, E.; De Sanctis, M.C.; Nathues, A.; Hiesinger, H.; Ammannito, E.; Raymond, C.A.; Jaumann, R.; Longobardo, A.; et al. The formation and evolution of bright spots on Ceres. *Icarus* **2019**, *320*, 188–201. [CrossRef]
35. Elbeshausen, D.; Wünnemann, K.; Sierks, H.; Vincent, J.B.; Oklay, N. The Effect of Topography on the Impact Cratering Process on Lutetia. In Proceedings of the Lunar and Planetary Institute Science Conference Abstracts, The Woodlands, TX, USA, 19–23 March 2012; p. 1867.
36. Russell, C.T.; Raymond, C.A.; Ammannito, E.; Buczkowski, D.L.; De Sanctis, M.C.; Hiesinger, H.; Jaumann, R.; Konopliv, A.S.; McSween, H.Y.; Nathues, A.; et al. Dawn arrives at Ceres: Exploration of a small, volatile-rich world. *Science* **2016**, *353*, 1008–1010. [CrossRef] [PubMed]
37. Fu, R.R.; Ermakov, A.I.; Marchi, S.; Castillo-Rogez, J.C.; Raymond, C.A.; Hager, B.H.; Zuber, M.T.; King, S.D.; Bland, M.T.; Cristina De Sanctis, M.; et al. The interior structure of Ceres as revealed by surface topography. *Earth Planet. Sci. Lett.* **2017**, *476*, 153–164. [CrossRef]
38. Castillo-Rogez, J.C.; Hesse, M.A.; Formisano, M.; Sizemore, H.; Bland, M.; Ermakov, A.I.; Fu, R.R. Conditions for the Long-Term Preservation of a Deep Brine Reservoir in Ceres. *Geophys. Res. Lett.* **2019**, *46*, 1963–1972. [CrossRef]
39. Castillo-Rogez, J.; Neveu, M.; McSween, H.Y.; Fu, R.R.; Toplis, M.J.; Prettyman, T. Insights into Ceres's evolution from surface composition. *Meteorit. Planet. Sci.* **2018**, *53*, 1820–1843. [CrossRef]
40. De Sanctis, M.C.; Ammannito, E.; Raponi, A.; Marchi, S.; McCord, T.B.; McSween, H.Y.; Capaccioni, F.; Capria, M.T.; Carrozzo, F.G.; Ciarniello, M.; et al. Ammoniated phyllosilicates with a likely outer Solar System origin on (1) Ceres. *Nature* **2015**, *528*, 241–244. [CrossRef] [PubMed]
41. De Sanctis, M.C.; Raponi, A.; Ammannito, E.; Ciarniello, M.; Toplis, M.J.; McSween, H.Y.; Castillo-Rogez, J.C.; Ehlmann, B.L.; Carrozzo, F.G.; Marchi, S.; et al. Bright carbonate deposits as evidence of aqueous alteration on (1) Ceres. *Nature* **2016**, *536*, 54–57. [CrossRef] [PubMed]
42. Ermakov, A.I.; Fu, R.R.; Castillo-Rogez, J.C.; Raymond, C.A.; Park, R.S.; Preusker, F.; Russell, C.T.; Smith, D.E.; Zuber, M.T. Constraints on Ceres' Internal Structure and Evolution From Its Shape and Gravity Measured by the Dawn Spacecraft. *J. Geophys. Res.* **2017**, *122*, 2267–2293. [CrossRef]
43. Bland, M.T.; Raymond, C.A.; Schenk, P.M.; Fu, R.R.; Kneissl, T.; Pasckert, J.H.; Hiesinger, H.; Preusker, F.; Park, R.S.; Marchi, S.; et al. Composition and structure of the shallow subsurface of Ceres revealed by crater morphology. *Nat. Geosci.* **2016**, *9*, 538–542. [CrossRef]
44. Krohn, K.; Neesemann, A.; Jaumann, R.; Otto, K.A.; Stephan, K.; Wagner, R.J.; Tosi, F.; Zambon, F.; Ruesch, O.; Williams, D.A.; et al. Ring-Mold Craters on Ceres: Evidence for Shallow Subsurface Water Ice Sources. *Geophys. Res. Lett.* **2018**, *45*, 8121–8128. [CrossRef]
45. Ruesch, O.; Platz, T.; Schenk, P.; McFadden, L.A.; Castillo-Rogez, J.C.; Quick, L.C.; Byrne, S.; Preusker, F.; O'Brien, D.P.; Schmedemann, N.; et al. Cryovolcanism on Ceres. *Science* **2016**, *353*, aaf4286. [CrossRef] [PubMed]